2017

Vibration-Assisted Convective Deposition of Binary Suspensions for Structured Coatings

Thitiporn Kaewpetch
Lehigh University

VIBRATION-ASSISTED CONVECTIVE DEPOSITION

OF BINARY SUSPENSIONS FOR STRUCTURED COATINGS

by

Thitiporn Kaewpetch

A Thesis

Presented to the Graduate and Research Committee of Lehigh University

in Candidacy for the Degree of

Master of Science

in

Polymer Science and Engineering Program,

Material Science and Engineering

Lehigh University

May 2017

CERTIFICATE OF APPROVAL

This thesis is accepted and approved in partial fulfillment of the requirements for the Master of Science.

_____

Date

_____

Prof. James F. Gilchrist

Thesis Advisor

_____

Prof. Wojciech Z. Misiolek

Chairperson of Department

Acknowledgement

First of all, I am truly grateful to my thesis advisor, Prof. James F. Gilchrist, for excellent guidance and great support throughout this research. It is my pleasure to join his research group. The Gilchrist group has provided me not only the knowledge and the research facilities to conduct the research, but also the companionship from everyone in this group, especially Kedar Joshi, and Zhiqiao Zeng.

I would like to thank to Royal Thai Government for the opportunity to study in the United States. Thanks to Thai students at Lehigh, especially Choat Inthawongse, and Thai families in Allentown for all your help and kindness since the first day I came here. Also, I would like to recognize my friends both from here and Thailand, for good support and suggestion. No matter what happened, they always stood by me and gave me their helpful opinion.

I would like to give special thanks to my family for their support and advise during the time in the United States. The support from the family is the main factor driving me to overcome the obstacle. Finally, I would like to dedicate this research to my aunt (my God mother) who just passed away as she is one of the most important persons in my life and she is the one who makes me want to follow my childhood dream (pursuing PhD).

Table of contents

List of Figures

Abstract

There are many applications for thin films of ordered particles including membranes, microlens arrays, and structure-color coatings. Convective deposition, a process that uses evaporation-driven flow in a thin liquid film to order particles, is a relatively fast and scalable method of making such films. Recently, it was shown that using lateral vibration in the direction of coating can enhance this process. This work focuses on depositing well-ordered monolayers of a binary suspension of microspheres and nanoparticles to understand the effect of the process parameters on the final distribution of particles. In order to investigate the deposited morphology of binary suspensions, various concentrations of nanoparticles were deposited on the substrate at 50 Hz frequency and a range of vibration amplitudes. The result was for all concentrations, the deposition rate and the range of speed for monolayers tend to increase with amplitude of vibration. The overall quality of the thin films is more uniform; the stripes are rarely seen. However, areas exist where microspheres were not surrounded by nanoparticles, and this inhomogeneity increases with higher amplitude vibration. To analyze the non-uniformity of deposition, samples were imaged using confocal laser scanning microscopy and particle-level image analysis. The particle coverage, the intensity of segregation, the distribution of number of nearest neighbored particles of microsphere and local area of particles were characterized. At low amplitude, the nanoparticle coverage is higher and has small deviation over large sample areas. As expected, each microsphere on average has 6 nearest neighbored (NN) particles and a relatively uniform local area distribution for uniform, well-ordered particle coatings. On the other hand, when the coverage has many defects due to vibration, the average number of NN particles tends to decrease which can also be described by the a

decrease in the distribution of local areas. Even though many localized defects are generated when vibration is imposed, the overall uniformity remains high, as indicated by a low intensity of segregation across all vibration samples. All of these parameters allow a direct connection of microstructure to the macroscopic process parameters.

1. Introduction

Convective deposition, the flow-assisted self-assembly driven by an evaporative flux, has potential for designing nanoscale structures for many fields varying from nanotechnology for electronic devices, such as enhancement of microlens arrays for light emitting diodes[1–6], to biotechnology for pharmaceutical and biomedical applications, such as biocoating from live cell-particle suspensions[7,8], surface-enhanced Raman scattering by cells of microorganism[9], and membranes for bioseparations[10]. This process has the ability to fabricate 3D-structured coatings using a continuous, scalable process.

Convective deposition is a rapid, inexpensive, and easily controlled method for creating self-assembled, ordered particle monolayer coatings. It was developed from observations of spontaneous crystallization in thin films. In those experiments, two fundamental mechanisms in thin film colloidal crystallization of colloidal particle assembly are nucleation, driven by the capillary forces between the particles, and the crystal growth governed by the water evaporation from the already ordered area (figure 1). [11–13] This can occur when a colloidal suspension is spread over a substrate. After water evaporation, the thickness of the liquid layer gradually decreases to the particle diameter and the crystal nuclei are suddenly formed under the attractive capillary forces. When the particles are partially immersed in the thin liquid layer, the liquid-air interface is deformed. To minimize the surface energy, strong interparticle capillary forces arise and allow the crystal to grow by particle-particle and particle-substrate attractions at the contact line.

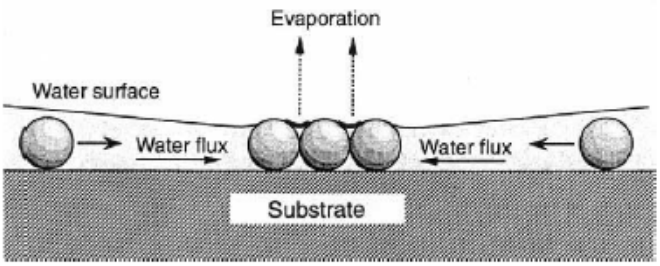

Figure 1 Schematic process of particle assembly governed by liquid flow.[12]

Instead of random nucleation and growth, it is possible to utilize these physics to fabricate perfect colloidal monolayers. Nagayama and his colleague proposed a simple mass balance to estimate the withdrawal velocity of the substrate plate, v_s, which must be equal to the crystal formation rate, v_c, as following equation.[13]

$$v_s = v_c = \frac{\beta l}{0.605} \frac{J_e \phi}{Nd(1-\phi)} \quad (1)$$

The crystal formation rate, v_c, depends on the particle volume fraction, ϕ, evaporation flux of the liquid medium, J_e, drying length, l, particle diameter, d, layers of particle array, N, and a deposition parameter, β. Here, β varies from 0 to 1, depending on particle-particle and particle-substrate interactions. Three resulting morphologies of deposited particles are sub-monolayer, monolayer, and multilayer, are presented (figure 2). These morphologies are dependent on the relationship of v_s to v_c. The ideal deposited monolayer is formed when $v_s = v_c$ (figure 2b). If $v_s < v_c$, it results in sub-monolayer (figure 2a); otherwise, multilayer appears when $v_s > v_c$ (figure 2c), where it is possible to create many-layered colloidal crystals thin films.

Since these early studies, the convective deposition of mono-sized colloidal suspensions has been investigated many times over for many applications. One method to improve surface properties of the thin films applies the use of binary suspensions of different sizes of particles, microspheres and nanoparticles. The nanoparticles fill the interstitial spaces between the microspheres while reducing various defects and instabilities that can occur. Achieving well-ordered microsphere monolayers, an optimum ratio of volume fraction of nanoparticles to microspheres, ϕ_{nano}/ϕ_{micro}, was determined to balance the relative microsphere and nanoparticle fluxes during assembly. On the other hand, when ϕ_{nano} was lower or higher than the optimum value, ϕ^*_{nano}, an instability arised and caused the formation of stripes; alternating monolayer and sub-monolayer regions ($\phi_{nano} < \phi^*_{nano}$) or alternating monolayer and multilayer bands ($\phi_{nano} > \phi^*_{nano}$).[14] In case of insufficient nanoparticle flux, the moving of microspheres was faster than that of nanoparticle resulting in the stripe formation. Otherwise, when the nanoparticle flux was much greater than the flux of microsphere, the nanoparticles inhibited the crystallization of microspheres, sub-monolayers were formed, or the microspheres were vertically packed and formed multilayers.[15] Recently, vibration was employed in conventional convective deposition in order to enhance the morphology of the thin films.[16] This vibration-assisted convective deposition resulted in a faster speed of monolayer deposition and a larger range of monolayer speeds for an optimum concentration (20 vol% silica microspheres and 8 vol% nanoparticles).

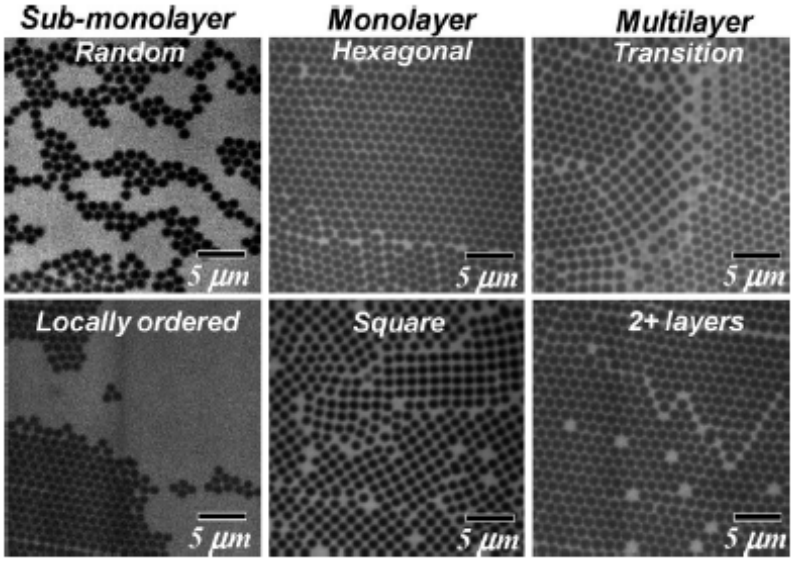

Figure 2 Three resulting morphologies of deposited particle layer: (a) sub-monolayer, (b) monolayer, and (c) multilayer.[4]

As stated above, the stripes were noticed at low volume fraction of nanoparticles. In this study, we aim to minimize the formation of stripes for samples with low nanoparticle content and improve nanoparticle distribution by using lateral substrate vibration-assisted convective deposition. The effect of amplitude, A_0, and frequency, ω, of vibration was considered in the previous work. [16] They found that the higher ω, especially ω = 50 Hz, resulted in the tremendously larger range of conditions for monolayer depositions and no limitation to small A_0. Thus we study the effect of A_0 on the morphology of the deposited films for low nanoparticle volume fractions at ω = 50 Hz. We observe the defect within the thin films (section 3.1), monolayer deposition speeds, v_{mono}, at different A_0 (section 3.2) and characterize the microstructure of deposited particle layers by image analysis (section 3.3).

2. Materials and Methods

2.1 Suspension Preparation

The primary aqueous colloid suspension used in this work is prepared by dispersing silica microspheres (Fiber Optic Center Inc., USA), having a density of 2.2 g/cm^3 and an average diameter of $2a_{micro}$ = 0.95 ± 0.02 μm, in deionized (DI) water at volume fraction ϕ_{micro}= 0.2. The suspension is dispersed using a sonic dismembrator (model 550, Fisher Scientific, Pittsburgh, PA) for 15 min. A separate colloidal suspension of diameter $2a_{nano}$= 100 nm polystyrene (PS) nanoparticles prepared at ϕ_{nano}=0.08 in DI water (supplied by the Emulsion Polymer Institute, Lehigh University) is combined with the silica solution to achieve the desired suspension composition.

2.2 Substrate Preparation

Plain glass microslides (76 × 25 × 1 mm^3, Fisher PA), and glass coverslips (40 × 24 × 0.25 mm^3, Fisher PA) are used as deposition blades and substrates, respectively. All glassware is cleaned by immersion in Piranha solution, 5:1 v/v sulfuric acid/hydrogen peroxide, for at least 3 hours. The cleaned glassware is rinsed with DI water until no residual acid remains and is then immersed in DI water until use. The bottom edge of the glass deposition blade is treated to be hydrophobic by adding a thin coating with parafilm (Fisher PA).

2.3 Deposition.

The experimental setup is shown in Figure 3. This apparatus is contained within a humidity-controlled environment, where all experiments were performed at a constant 20%

relative humidity and 24°C. The deposition blade angle is fixed at 45°, positioned approximately 10 μm above the substrate. The volume of 10 μl colloid suspension is injected into the wedge between the substrate and deposition blade for each experiment. The substrate is then pulled at a certain deposition speed (25 μm/s ≤ v_s ≤ 120 μm/s) using a linear motor (Harvard Instrument Co. Ltd.), while a mechanical driver (PASCO SF-9324) and a waveform generator (Agilent 3320A) are used to periodic oscillation. The position of the substrate is given by

$$x = v_s t + A_0 \sin\omega t, \tag{2}$$

where v_s is the apparent deposition velocity of the substrate and A_0 and ω are the amplitude and frequency of vibration. The effect of vibration at various A_0 and ω = 50 Hz is studied.

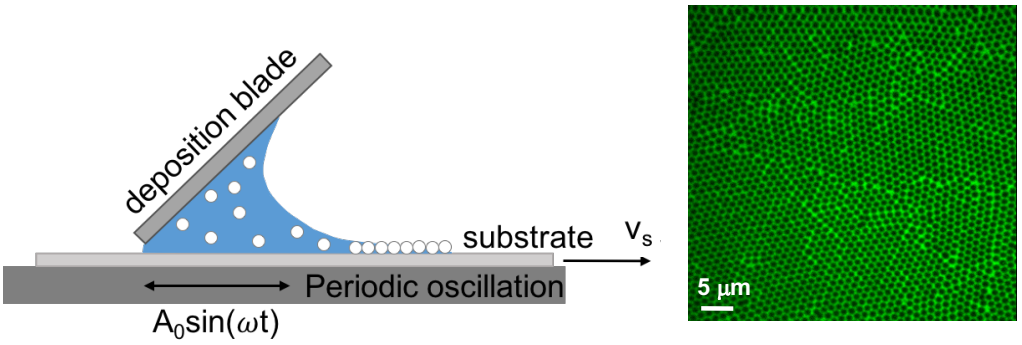

Figure 3 Left, schematic diagram of experimental setup showing deposition apparatus with periodically oscillating and moving substrate. Right, example image of deposited microspheres (black) and nanoparticles (green).

2.4 Microstructure Analysis

Deposited monolayers are observed directly using confocal laser scanning microscopy (VTeye, Visitech International). The sample is scanned along the deposition length sampling (~60000 microspheres). The relative microsphere substrate coverage, ρ, Intensity of segregation, I, the distribution of nearest neighbor microspheres, and the local area, where a central particle is surrounded by its nearest neighbor particles, are evaluated.

3. Results and Discussions

In this study, the effect of vibration amplitude, A_0, on the morphology of the deposited films for low nanoparticle volume fractions is reported. We observe the defects that form within the thin films (section 3.1) at monolayer deposition speeds, v_{mono}, at different A_0 (section 3.2) and characterize the microstructure of deposited particle layers by image analysis (section 3.3). Finally, we hypothesize the origin of these defects based on the evidence of the defect distribution.

3.1 Defects within the thin films

As mentioned above, in case of the optimal nanoparticle concentration, microspheres are completely surrounded by nanoparticles; nanoparticles fill the interstitial regions between microspheres. The stripes that form due to the flux imbalance occurs when lower than optimum nanoparticle concentrations are used. When vibration is employed in the system, the overall quality of the thin film is uniform; the stripes are rarely seen. However, at low nanoparticle concentrations, the defects, which are defined as areas where nanoparticles do not exist, occur with the use of vibration. The defects are represented as black areas in figure 4(b), 4(c), and 4(d). The amount of defects is dependent on the concentration and the amplitude of vibration, which will be characterized in section 3.3. Nevertheless, within the defect regions the microspheres have been locally ordered as seen in Figure 5. Thus well-ordered monolayer of microspheres could be expected although some regions lack nanoparticle. It will be presented in terms of deposition speed at various amplitudes of vibration (section 3.2).

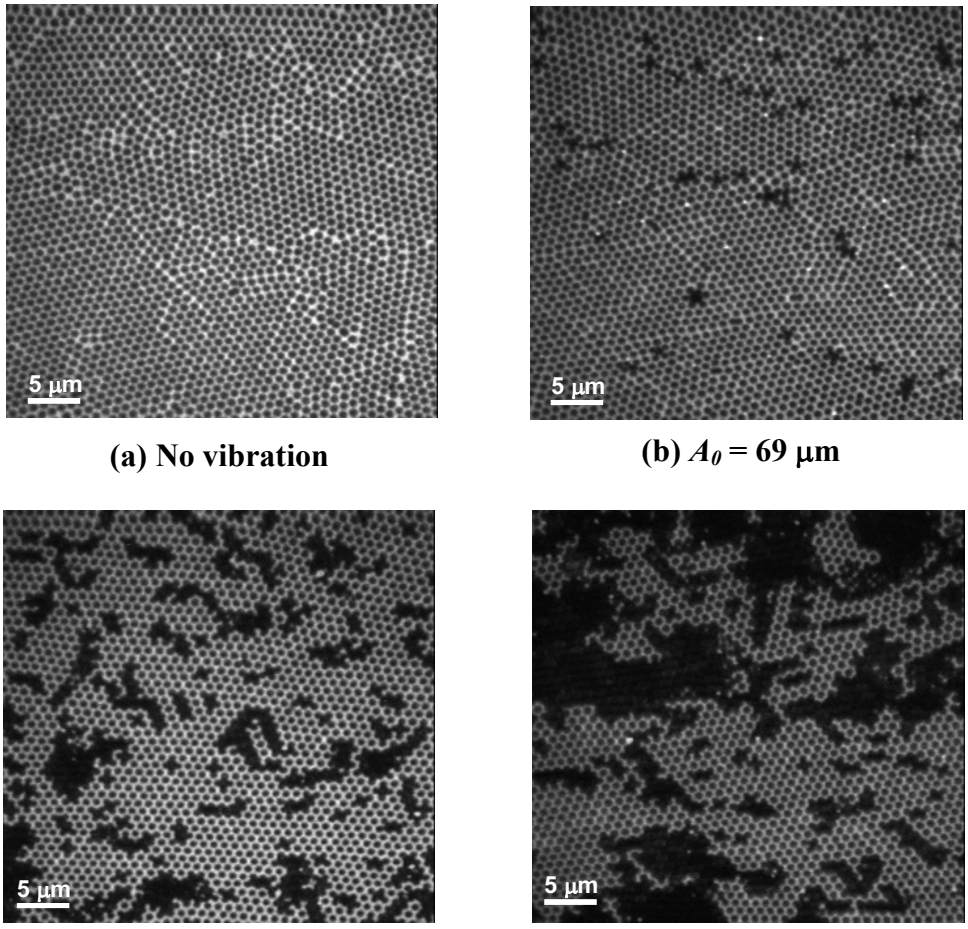

(a) No vibration **(b) A_0 = 69 μm**

(c) A_0 = 193 μm **(d) A_0 = 317 μm**

Figure 4 Scanned images for ϕ_{nano}:ϕ_{micro} = 0.01:0.2 from confocal laser scanning microscopy of which black dots and white background represent microspheres and nanoparticles, respectively. Defects occur after vibration is used. These defects are defined as area where nanoparticles do not exist.

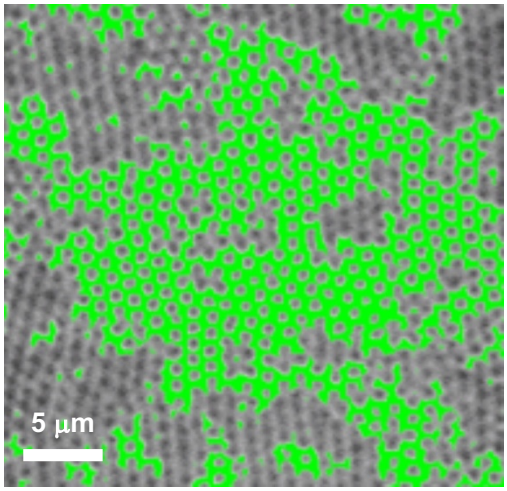

Figure 5 Dye-subtracted-scanned image from Confocal microscopy for ϕ_{nano}:ϕ_{micro} = 0.01:0.2 at 317μm amplitude. The microspheres within the defect regions are shown. Green areas represent non-defect regions and grey areas are defect regions.

3.2 Morphologies and the deposition speeds of the thin films

Figure 6 shows the morphologies of thin films after depositing at various deposition speeds and amplitudes of vibration. As seen in previous research, without vibration, A_0 = 0, there is a very narrow range of deposition speed that results in monolayer coatings.[15,16] With added vibration, v_{mono} increases with the amplitude of vibration, A_0. This can be interpreted as either the evaporation rate, J_e, or the drying length, l, increases when the amplitude is increased. Surpisingly, a wide range of deposition speeds that result in monolayer morphology is also observed at higher vibration amplitudes as compared to deposition without the use of vibration. These results agree well with the previous research which studied at an optimum nanoparticle volume fraction, ϕ_{nano} = 0.08; the addition of vibration enhances the monolayer speed of deposition.[16] When the substrate is subjected to horizontal vibration, especially ultrasonic vibration at low A_0 and high ω, the horizontal vibration can create waves which lead to an increase in interface between the air and the

liquid film, thus the evaporation rate is faster.[17] Likewise, this low-amplitude vibration can enhance the film uniformity.[18–21] In this study, a description of the drying length, l, is much more complicated because added inertia resulting from vibration. The relative amount of inertia in this system is characterized by the Weber number, We, which is the ratio of the drop inertia to the surface tension,

$$We = \frac{\rho A_0 \omega^2 L^2}{\gamma} \tag{3}$$

where ρ is density of fluid, A_0 is vibration amplitude, ω is frequency, L is radius of curvature of the droplet between the blade and substrate, and γ is surface tension. In this case, based on millimeter scale of L, We value is between $O(10^{-1})$ and $O(1)$, demonstrating that inertia is roughly significant, but much less than ultrasonic vibration. In these experiments with moderate to large A_0 and low ω, the increase in evaporation rate is likely associated with a change in the length associated with the drying film, l. It has been hypothesized that the particle-substrate lubrication interactions may play a role in this deposition rate.

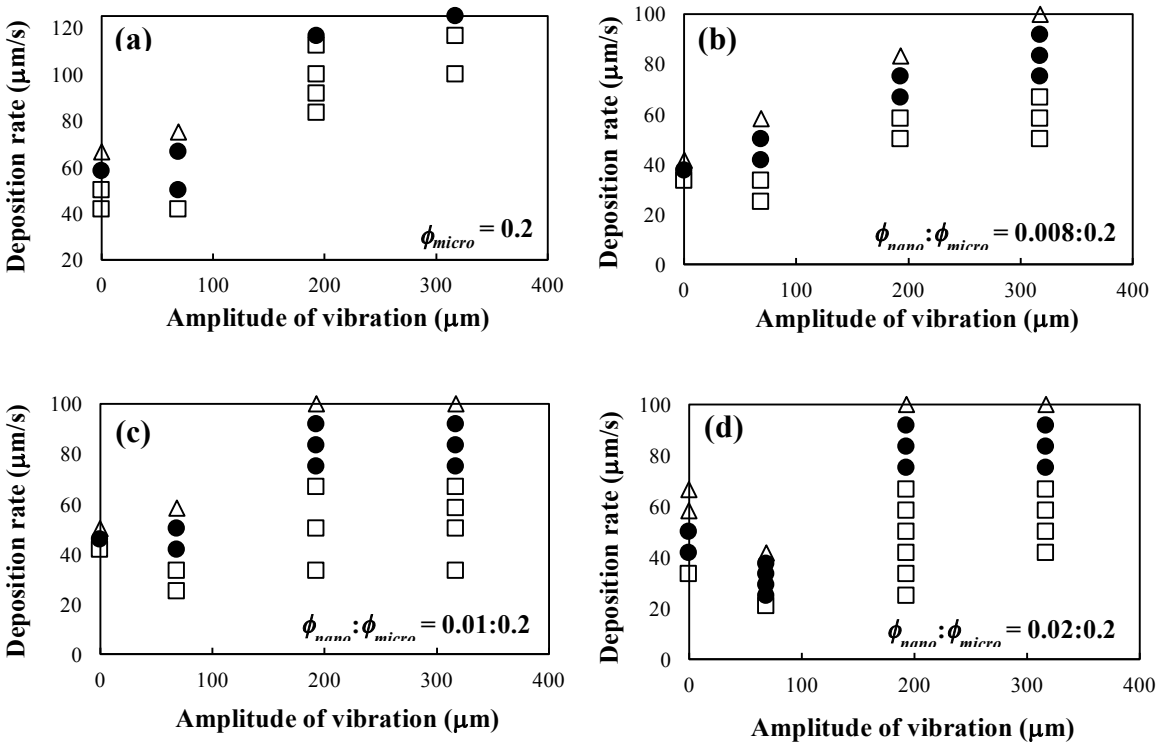

Figure 6 Phase diagram show resulting morphologies as a function of changing amplitude of vibration and deposition speed for (a) $\phi_{micro} = 0.2$ (b) $\phi_{nano}:\phi_{micro} = 0.008:0.2$ (c) $\phi_{nano}:\phi_{micro} = 0.01:0.2$ and (d) $\phi_{nano}:\phi_{micro} = 0.02:0.2$. Open triangles represent submonolayer morphologies, black circles are monolayer morphologies, and open squares are multilayer morphologies.

In monosized suspensions (Figure 6a), v_{mono} is apparently higher than that of binary suspensions (Figure 6b-d). From the Nagayama relationship, one may deduce that addition of nanoparticles may increase v_s but the results show that the deposition speed decreases after the addition of nanoparticles. This lower speed likely results from a lower evaporation rate because of the available area for evaporation and the presence of nanoparticles depressing the vapor pressure of the solvent. However, another possible assumption is that the drying length, l is affected by the addition of nanoparticles. The drying length, l, in Eq. (1) is generally assumed to be constant. It is used to estimate coating thickness, h, in only

small range of substrate velocities. Recently, Nagayama equation Eq. (1) has been modified by Joshi and Gilchrist[22] in order to predict *l* and *h* over a larger range of substrate velocities, v_s, for non-vibrated systems.

3.3 Effect of vibration on thin film microstructure

3.3.1 The relative degree of microsphere substrate coverage (ρ) and intensity of segregation (I)

The particle coverage, ρ, can be utilized to characterize the overall particles distribution within the thin film. It is defined as exactly found microspheres, N_f, over total possible microspheres within scanned area, N_t.

$$\rho = \frac{N_f}{N_t} \tag{4}$$

For all concentrations, ρ within the scanned area tends to decrease at higher amplitude of vibration, A_0 (red and green data in figure 7). The deviation of coverage, σ, increases significantly when less nanoparticles are present (figure 8). Moreover, σ is larger at high vibration amplitude. These are a measures of the non-uniformity of thin film, representing the prominence of defects in the samples, as shown in Figure 4d.

The amount of nanoparticle coverage of the microspheres depends on ϕ_{nano}.[14] Without the use of vibration, the samples $\phi_{nano} < 0.06$ have patchy regions where interstitial spaces between microspheres are completely filled with nanoparticles; other regions have microspheres with sparsely distributed nanoparticles (figure 9a). However, fluorescence imaging using confocal laser scanning microscopy shows only the regions where microspheres are surrounded by nanoparticles (figure 4a). The possible reason for non-uniform thin film might be that the large instability of interface between the air and the

contact line occurs when very high-amplitude of vibration is imposed. This instability may tremendously affect the pressure distribution inside the capillary flow through the deposited microspheres which causes the local obstruction of nanoparticles in the interstitial regions.

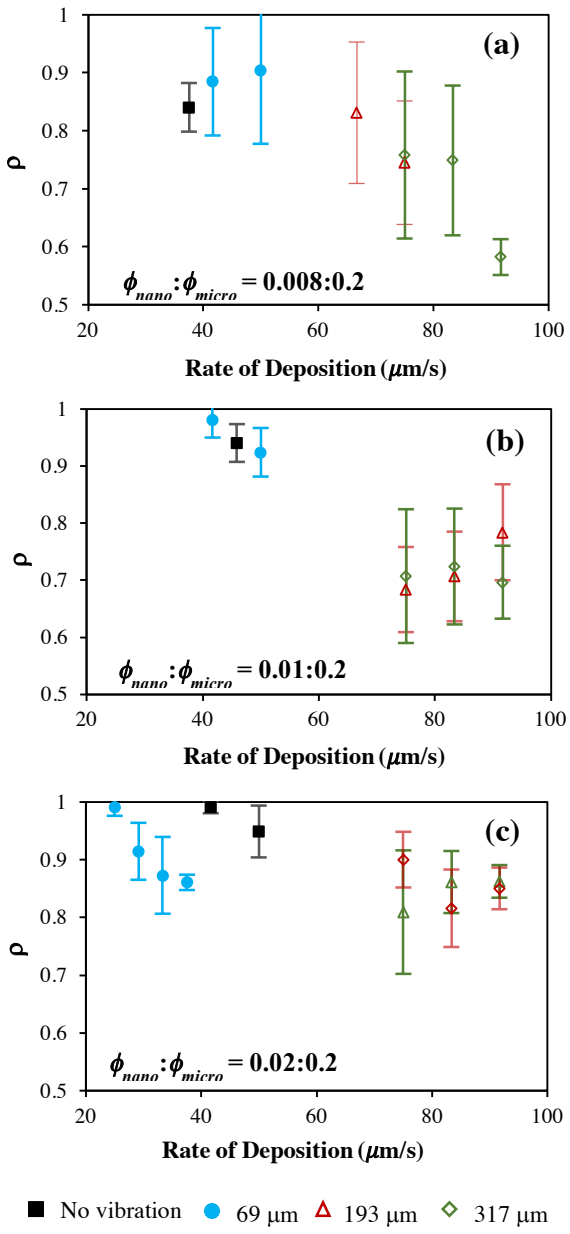

Figure 7 Particle coverage, ρ, of the thin film samples, which is defined as exactly found microspheres over total possible microspheres within scanned area.

Moreover, when nanoparticle concentration is lower than an optimal value, the nanoparticle flux is deficient and it causes the moving front of nanoparticles to lag behind that of microspheres. Instability arises and causes the meniscus to jump.[15] Therefore, for samples $\phi_{nano} < 0.02$ with vibration, some patchy areas might not have nanoparticles; black areas appear (figure 4b, 4c, and 4d). Especially, at high vibration amplitudes (193 μm and 317 μm), these defects emerge throughout the sample but some areas have small and some have large defects. Thus σ of the samples at intense vibration are apparently large.

Very small values of σ are observed for several samples at high monolayer deposition speeds and vibration since high speed and vibration lead to roughly equal-sized defects throughout the samples. Furthermore, at high volume fraction the dynamics of the system slows down and the time scale for the segregation mechanism could become larger.[23] Hence the samples with higher nanoparticle concentration (ϕ_{nano}:ϕ_{micro} = 0.02:0.2) have the smallest σ values (figure 8).

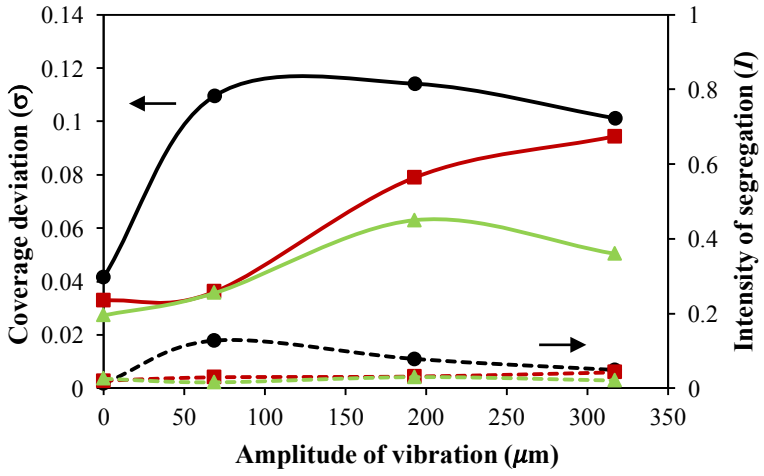

Figure 8 Standard deviation, σ, (solid line) and intensity of segregation, I, (dash line) of particle distribution within the thin deposited films at various compositions of ϕ_{nano}: ϕ_{micro} = 0.008:0.2 (●), 0.01:0.2 (■), and 0.02:0.2 (▲)

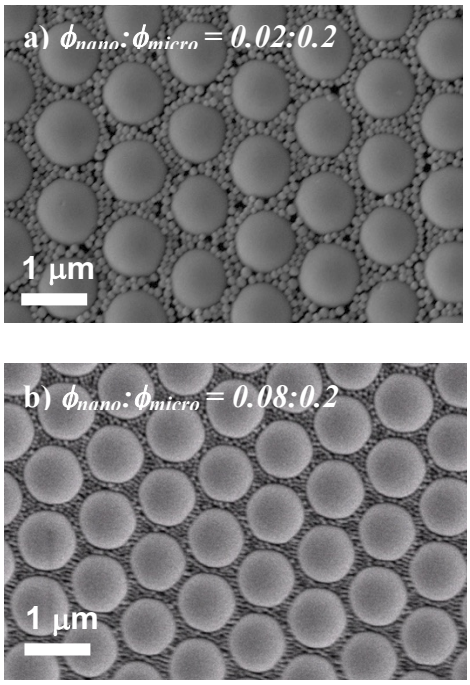

Figure 9 SEM images for a) ϕ_{nano}:ϕ_{micro} = *0.02:0.2* and b) ϕ_{nano}:ϕ_{micro} = *0.08:0.2* at non-vibrational operation.

To analyze the uniformity of the system, the intensity of segregation, *I*, is generally used and quantified by the following mathematic expression, [24]

$$I \equiv \frac{\sigma_\rho^2}{\bar{\rho}(1-\bar{\rho})} \tag{5}$$

where $\bar{\rho}$ is mean particle coverage, and σ_ρ^2 are the variances of particle coverage. When segregation is complete, *I* is equal to 1 and when the thin film is uniform, *I* is equal to 0. Although the number of defects tends to increase when nanoparticle concentrations decrease or the amplitude of vibration is much intense; σ is larger, the values of *I* are very low (~ 0.02 - 0.12), indicating that the defects appear uniformly throughout the thin film.

3.3.2 The distribution of nearest neighbor particles

The distribution of nearest neighbor (NN) particles is another method to characterize the homogeneity of thin film. The number of NN is quantified from the pair-correlation function $g(\vec{r})$ which is widely used to investigate the structure of isotropic random packing. $g(\vec{r})$ is proportional to the probability of finding a sphere center inside the area at a distance $\vec{r}$ from a given sphere center.[25,26] Theoretically, the microspheres, which are hexagonally well ordered, have six NN particles. They can have a bit higher or lower than six NNs when they are slightly disordered. Otherwise, when the microspheres are adversely disoriented, the number of the nearest neighbors decreases significantly.

For all samples examined in this study, the probability, *P*, having six NNs, is obviously high for the samples without vibration. This is also apparent for the lowest degree of vibration considered, A_0 = 69 μm, shown in figure 8 (black and blue lines). On the contrary, when strong vibration amplitudes (193 μm and 317 μm) are used, *P* decreases due to non-uniformity of thin film as shown in figure 8 (red and green lines). However, the probability is slightly higher for samples with A_0 = 317 μm (green line) than A_0 = 193 μm (red line) because the defect areas are equally larger throughout the sampling regions comparing to the defect areas of samples conducted at lower amplitude (figure 2d). This can be linked to small σ values observed at A_0= 317 μm. Since the strong vibration leads to non-uniformity of thin film, the number of NN decreases. The probability having 2 to 5 NNs increases, corresponding to the lower *P* of having 6 NNs. The graph becomes noticeably broader (figure 10), especially at higher vibration amplitudes (193 μm and 317 μm).

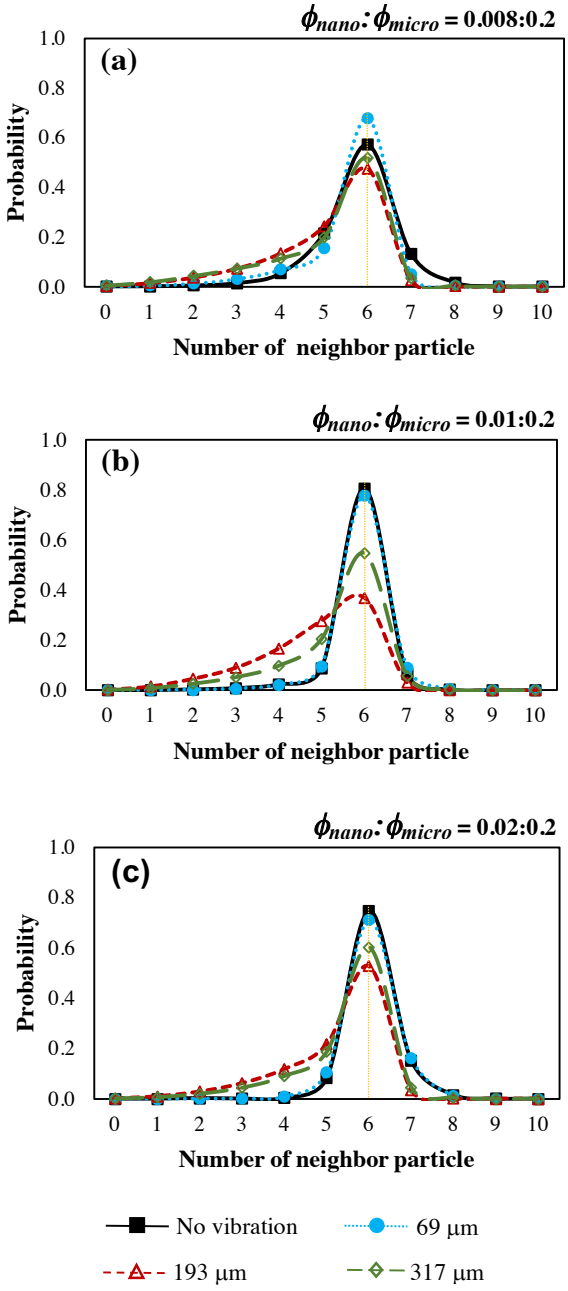

Figure 10 The probability distribution of nearest neighbor particle. For a perfect crystal, a central particle has six nearest neighbors.

3.3.3 The distribution of local area of the thin films

The number of nearest neighbors is used to characterize only the uniformity of the thin films but local area can be used to analyzed both the uniformity and how well the microspheres are ordered. The local area, A, is given as

$$A = 2a^2 \sum_{i=0}^{n} sin(\theta_i) \quad (6)$$

This area A depends on the number of nearest neighbors, n, the distance between the central particle and the nearest neighbors, a, and the angle between two adjacent nearest neighbors, θ. If the microspheres are perfectly hexagonally ordered, the minimum local area, A_{min}, for each microsphere is about 2.6 μm^2.

Figure 11 shows the distribution of the local area of each microsphere within the thin film. The average local areas, highest peaks in the distribution, are weakly depend on the amplitude of vibration between 2.9 $\mu m^2 \leq A \leq 3.2$ μm^2. Similar to the distribution of nearest neighbors, the probability, P, to achieve the area of 2.9 $\mu m^2 \leq A \leq 3.2$ μm^2 is very high for the samples without or with the use of small vibration, as shown in figure 11 (black and blue lines). Nonetheless, P decreases; the peaks significantly shift lower, with increasing amplitude of vibration as shown in figure 11 (red and green lines). Also, a small second peak is observed for the samples with strong vibration indicating that the number of microspheres having small local areas (~1.5 μm^2) tend to increase with amplitude of

vibration. These happen due to the non-uniformity of the thin film which is corresponding to the smaller ρ and larger σ values at high vibration amplitudes.

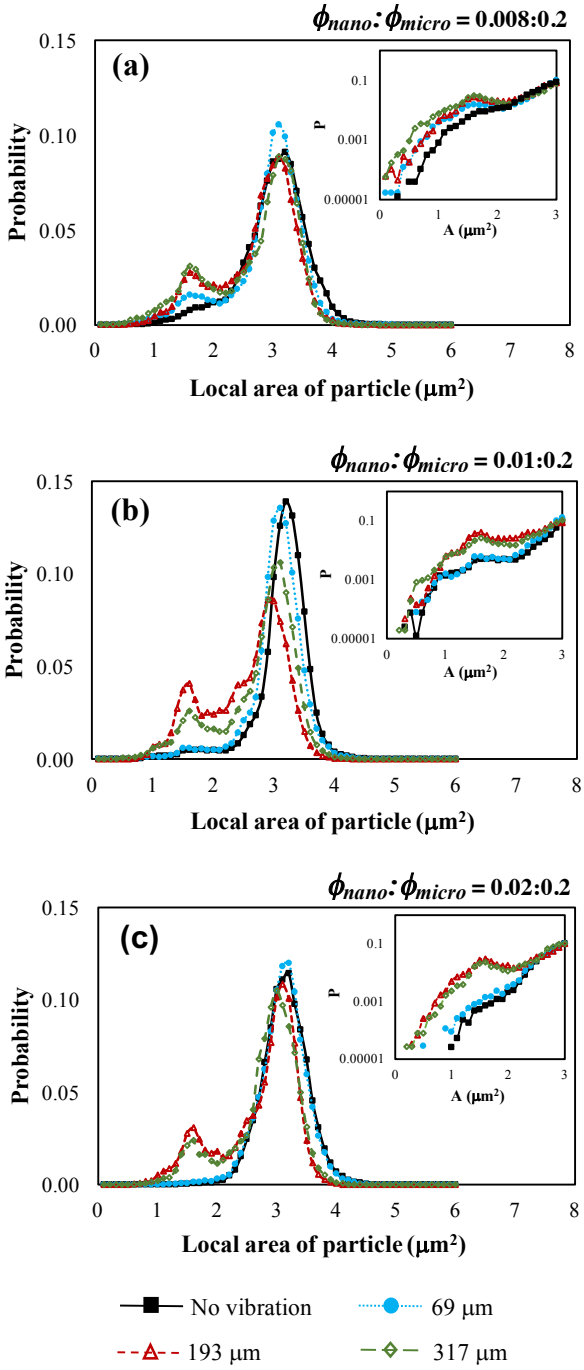

Figure 11 The probability distribution of local area of each microsphere at various amplitudes of vibration. The local area is defined as the area within the connection of nearest neighbors. It is about 2.6 μm^2 when microspheres are in perfect order.

In addition, the peak slightly shifts closer to A_{min} (~2.6 μm^2) when the vibration is stronger. This could be implied that the microspheres are better ordered with the use of vibration. However, using strong vibration may lead to disordered packing of microspheres; the average local areas slightly increase for very low concentration of nanoparticles (ϕ_{nano} = 0.008 and 0.01) as shown in figure 11 (green line). From the results, the average local areas are not exactly the same as A_{min}. This may not be only because of disordered packing but electrostatic repulsion between microspheres as well.[27]

4. Conclusions and future work

The vibration-assisted convective deposition enhances the deposited monolayers for the suspensions with both optimal concentration (ϕ_{nano}:ϕ_{micro} = 0.08:0.2)[12] and, as shown in this work, low nanoparticle concentrations (ϕ_{micro} = 0.2 and ϕ_{nano} = 0.008, 0.01, and 0.02). The formation of stripes is reduced after the vibration is imposed. However, areas developed where microspheres were not surrounded by nanoparticles, and this inhomogeneity increases with higher amplitude vibration. To analyze the non-uniformity of deposition, the particle coverage, the intensity of segregation, the distribution of number of nearest neighbored particles of microsphere and local area of particles were characterized. At low amplitude of vibration, the particle coverage is higher and has small deviation over large sample areas. As expected, each microsphere on average has 6 nearest neighbor (NN) particles and a relatively uniform local area distribution (~ 3 μm^2) for uniform, well-ordered particle coatings. On the other hand, when the coverage has many defects due to vibration, the average number of NN particles tends to decrease, and these defects result in smaller average local areas (~ 1.5 μm^2). Even though many defects

generate when vibration is imposed, the overall intensity of segregation is very low, indicating that the thin film is relatively uniform.

The conventional convective deposition has been potentially employed in various applications as well as coatings having embedded fibers. Cellulose fibers are biodegradable materials and have been widely used to improve many properties of materials but orientation of the fibers is needed to be considered. To get good orientation of fibers, convective deposition could be one of the powerful methods to orient the fibers. Cellulose suspensions have yield stress that must be overcome to shear the material during coating. To overcome the yield stress, vibration-assisted convective deposition could be a feasible way to break the yield stress to form engineered cellulose coatings.

References

(1) Arrays, C. T. M.; Li, X.; Zhu, P.; Liu, G.; Zhang, J.; Song, R.; Ee, Y.; Kumnorkaew, P.; Gilchrist, J. F.; Tansu, N. Light Extraction Ef Fi Ciency Enhancement of III-Nitride Light-Emitting Diodes by Using 2-D. **2013**, *9* (5), 324–332.

(2) Ee, Y. K.; Kumnorkaew, P.; Arif, R. A.; Tong, H.; Zhao, H.; Gilchrist, J. F.; Tansu, N. Optimization of Light Extraction Efficiency of III-Nitride LEDs with Self-Assembled Colloidal-Based Microlenses. *IEEE J. Sel. Top. Quantum Electron.* **2009**, *15* (4), 1218–1225.

(3) Ee, Y.-K.; Arif, R. A.; Tansu, N.; Kumnorkaew, P.; Gilchrist, J. F. Enhancement of Light Extraction Efficiency of InGaN Quantum Wells Light Emitting Diodes Using SiO[sub 2]/polystyrene Microlens Arrays. *Appl. Phys. Lett.* **2007**, *91* (22), 221107.

(4) Kumnorkaew, P.; Ee, Y. K.; Tansu, N.; Gilchrist, J. F. Investigation of the Deposition of Microsphere Monolayers for Fabrication of Microlens Arrays. *Langmuir* **2008**, *24* (21), 12150–12157.

(5) Ee, Y.-K.; Kumnorkaew, P.; Arif, R. a; Tong, H.; Gilchrist, J. F.; Tansu, N. Light Extraction Efficiency Enhancement of InGaN Quantum Wells Light-Emitting Diodes with Polydimethylsiloxane Concave Microstructures. *Opt. Express* **2009**, *17* (16), 13747–13757.

(6) Li, X. H.; Song, R.; Ee, Y. K.; Kumnorkaew, P.; Gilchrist, J. F.; Tansu, N. Light Extraction Efficiency and Radiation Patterns of III-Nitride Light-Emitting Diodes with Colloidal Microlens Arrays with Various Aspect Ratios. *IEEE Photonics J.*

2011, *3* (3), 489–499.

(7) Jenkins, J.; Flickinger, M.; Velev, O. Continuous Convective-Sedimentation Assembly of Colloidal Microsphere Coatings for Biotechnology Applications - Supplement. *Coatings* **2013**, *3* (1), 26–48.

(8) Jerrim, L. B.; Velev, O. D. Deposition of Coatings from Live Yeast Cells and Large Particles By "convective-Sedimentation" assembly. *Langmuir* **2009**, *25* (10), 5692–5702.

(9) Kahraman, M.; Yazici, M. M.; Şahin, F.; Çulha, M. Convective Assembly of Bacteria for Surface-Enhanced Raman Scattering. *Langmuir* **2008**, *24* (3), 894–901.

(10) Weldon, A. L.; Kumnorkaew, P.; Wang, B.; Cheng, X.; Gilchrist, J. F. Fabrication of Macroporous Polymeric Membranes through Binary Convective Deposition. *ACS Appl. Mater. Interfaces* **2012**, *4* (9), 4532–4540.

(11) Denkov, N.; Velev, O.; Kralchevski, P.; Ivanov, I.; Yoshimura, H.; Nagayama, K. Mechanism of Formation of Two-Dimensional Crystals from Latex Particles on Substrates. *Langmuir* **1992**, *8* (12), 3183–3190.

(12) Denkov, N. D.; Velev, O. D.; Kralchevsky, P. a.; Ivanov, I. B.; Yoshimura, H.; Nagayama, K. Two-Dimensional Crystallization. *Nature*. 1993, pp 26–26.

(13) Dimitrov, A. S.; Nagayama, K. Continuous Convective Assembling of Fine Particles into Two-Dimensional Arrays on Solid Surfaces. *Langmuir* **1996**, *12* (5), 1303–1311.

(14) Kumnorkaew, P.; Gilchrist, J. F. Effect of Nanoparticle Concentration on the Convective Deposition of Binary Suspensions. *Langmuir* **2009**, *25* (11), 6070–

6075.

(15) Kumnorkaew, P.; Weldon, A. L.; Gilchrist, J. F. Matching Constituent Fluxes for Convective Deposition of Binary Suspensions. **2010**, *26* (16), 2401–2405.

(16) Muangnapoh, T.; Weldon, A. L.; Gilchrist, J. F. Enhanced Colloidal Monolayer Assembly via Vibration-Assisted Convective Deposition. *Appl. Phys. Lett.* **2013**, *103* (18).

(17) Rahimzadeh, A.; Eslamian, M. Stability of Thin Liquid Films Subjected to Ultrasonic Vibration and Characteristics of the Resulting Thin Solid Films. *Chem. Eng. Sci.* **2017**, *158* (August 2016), 587–598.

(18) [6]Eslamian, M. Ultrasonic Substrate Vibration-Assisted Drop Casting (SVADC) for the Fabrication of Photovoltaic Solar Cell Arrays and Thin-Film Devices. *Nanoscale Res. Lett.* **2015**, 0–4.

(19) Zabihi, F.; Eslamian, M. Substrate Vibration-Assisted Spray Coating (SVASC): Significant Improvement in Nano-Structure, Uniformity, and Conductivity of PEDOT:PSS Thin Films for Organic Solar Cells. *J. Coatings Technol. Res.* **2015**, *12* (4), 711–719.

(20) Wang, Q.; Eslamian, M. Improving Uniformity and Nanostructure of Solution-Processed Thin Films Using Ultrasonic Substrate Vibration Post Treatment (SVPT). *Ultrasonics* **2016**, *67*, 55–64.

(21) Zabihi, F.; Ahmadian-Yazdi, M.-R.; Eslamian, M.; Heo, J.; Hyuk, S.; Noh, J.; Mandal, T.; Lim, C.; Chang, J.; Qinglong, J.; et al. Fundamental Study on the Fabrication of Inverted Planar Perovskite Solar Cells Using Two-Step Sequential Substrate Vibration-Assisted Spray Coating (2S-SVASC). *Nanoscale Res. Lett.*

2016, *11* (1), 71.

(22) Kedar Joshi, J. G. Estimation of Drying Length during Particle Assembly by Convective Deposition. *J. Colloid Interface Sci.* **2017**, *1*, 222–227.

(23) Peppin, S. S. L.; Elliott, J. a. W.; Worster, M. G. Solidification of Colloidal Suspensions. *J. Fluid Mech.* **2006**, *554* (1), 147.

(24) Danckwerts, P. V. The Definition and Measurement of Some Characteristics of Mixtures. *Appl. Sci. Res. Sect. A* **1952**, *3* (4), 279–296.

(25) Jullien, R.; Jund, P.; Caprion, D.; Quitmann, D. Computer Investigation of Long-Range Correlations and Local Order in Random Packings of Spheres. *Phys. Rev. E* **1996**, *54* (6), 6035–6041.

(26) Varadan, P.; Solomon, M. J. Direct Visualization of Long-Range Heterogeneous Structure in Dense Colloidal Gels. *Langmuir* **2003**, *19* (3), 509–512.

(27) Gilchrist, J. F.; Chan, A. T.; Weeks, E. R.; Lewis, J. a. Phase Behavior and 3D Structure of Strongly Attractive Microsphere-Nanoparticle Mixtures. *Langmuir* **2005**, *21* (24), 11040–11047.

Vita

Thitiporn Kaewpetch was born in August 1991 in Saraburi province, Thailand. She was raised by her aunt, Janfong Reunjan, in Saraburi. She attained elementary school at Anuban Saraburi school until grade 6. Then she moved to Bangkok to stay with her parents and completed high school at Surasakmontri school in 2010. She received her Bachelor degree in Food Technology, Faculty of Science, at Chulalongkorn University in 2014. During the same year, she got a scholarship from Thai government to study Master degree in the United States. She attained Lehigh in Fall 2015 in Polymer Science program, department of Material Science and Engineering. She has joined Prof. Gilchrist's research group in Chemical and Biomolecular Engineering since then.